Heat Affected Zone in the Wire Electrode During Electronic Flame Off in Bonding

Srinivas S. Sripada, I. M. Cohen, P. S. Ayyaswamy, L. Medalla, and B. J. Mulada
Department of Mechanical Engineering and Applied Mechanics
University of Pennsylvania
Philadelphia, Pennsylvania 19104-6315
Phone: 215-898-8362
Fax: 215-573-6334
e-mail: ayya@seas.upenn.edu

Abstract

In the wirebonding process process of microelectronic packaging, electric discharge heating is the first step. Typically, the discharge occurs between two electrodes, one element is a wire cylinder (anode) and the other element is a flat plate (cathode). The heat of the discharge causes the wire electrode tip to melt. Surface tension causes the molten metal to roll up into a ball. When a sufficient amount has melted, the discharge is terminated and the molten ball is allowed to solidify. Subsequently, the tip material is bonded to the chip bond pad. The wire spooled out through a capillary is looped over to form a second bond to the lead frame. Subsequently, the wire is torn off and, typically, the wire electrode is left with a bent tip, and the electronic flame off (EFO) process is repeated for the next pair of bonds. In this paper, the ball formation process is experimentally simulated using an up-scaled (60 x) model with a copper wire (1.55 mm diameter) having a bent tip. The discharge occurs in a 90 OCV arc chamber operating at a vacuum of 10-15 mm Hg with air as cover gas. The control variables are current, voltage, arc duration, arc gap, and chamber pressure. Thermocouples embedded in the wire are used to obtain the transient temperature variation. This temperature history is then used to deduce the heat transfer from the arc to the wire by solving the unsteady energy equation subject to appropriate boundary conditions. The Laplace transform technique is used for this purpose. Microscopic grain boundary studies of the solidified tips are carried out to ascertain the nature of solidification, the extent of porosity, and the heat affected zone (HAZ) in the wire electrode. Results for the transient current-power characteristics and the heat transfer are presented along with those for the metallographic studies. Based on such studies, optimal characteristics of initial tip shapes may be developed which influence the design of the capillary and the reliability of the joint. In fine pitched packaging, low loops of the wire interconnect are essential. The shape and the height of the loop is determined by the HAZ and this has motivated the current study.The formation of balls with minimum departure from sphericity, low porosity, along with a small HAZ is a challenge still faced in the industry.

Key words:

Fine pitch ball-bonding, Electronic Flame Off (EFO), Heat affected zone, Experimental scale up,
and Heat transfer.

1. Introduction

The wirebonding packaging process uses an EFO discharge between two electrodes causing a portion of one of them (the cylindrical wire anode) to melt, roll up into a ball, and later solidify. Specifically, an important part of Very Large Scale Integrated (VLSI) circuit chip assembly and packaging is the process of making electrical interconnections between the chip and a lead frame, which is ultimately connected to the other external electrical components. The most effective method of achieving this interconnection is the ball-wedge bonding process[1] which consists of the ball bonding step at one end of the interconnec-

© International Microelectronics And Packaging Society

tion and the wedge bonding step at the other end. The interconnection is made using a very fine metal wire (~25µm in diameter). The process involves melting the tip of the wire with an electrical discharge that is struck between the wire (anode) and a flat plate (cathode). The discharge process is commonly known in the industry as Electronic Flame Off (EFO). As the melting progresses, the molten wire rolls up by surface tension and forms a liquid sphere which grows in size until the discharge is terminated. This is followed by solidification of the spherical melt due to heat loss by conduction up the wire and to the surroundings. The resulting spherical tip is then ultrasonically (or thermosonically) bonded to the chip. The entire process has a duration of a few milliseconds. Then, the wire is wedge bonded to the chip's lead frame at a prescribed length from the ball. The length of wire between the two bonds is kept at a minimum so as to have the smallest possible chip profile as this length forms a loop from the bond pad on the chip to the lead frame. The height of this loop is affected by the length of the Heat Affected Zone (HAZ) along the wire axis from the ball. The length of the heat affected zone (HAZ) in the wire anode depends on the magnitude of the conductive heat flux along the axis of the wire during the EFO discharge process. The HAZ tends to be more brittle than the unaffected zone. The wire is looped (beyond the HAZ) and a second bond is made on the mounting lead frame, ultrasonically (without melting). Subsequently, the wire is torn off and the end is hooked from the deformation caused during the second bond. The EFO process is then repeated, starting from this hooked end.

Good balls are characterized by minimum departure from sphericity and low porosity that ensure good bond quality and therefore a secure interconnection. Much work has been done on wirebonding with nonprecious metals[2-13] . These studies have all been on the real (25 µm) scale. Harman[14] has provided an excellent compendium of factors affecting the strength and durability of wirebonds. The experimental and theoretical studies of the authors on ball formation[15-26] have helped make significant advances in modeling the discharge and subsequent ball formation process.

In this study, the researchers report discharge current and power characteristics, temperature transients, heat transfer calculations, and metallographic studies using a copper wire anode in a large scale model to assess the heat affected zone (HAZ).

2. Theory

The most important parameters governing the melting and resolidification of the anode tip are the wire diameter (d), the discharge current (I), the voltage drop (ΔV), the gap (G) between the electrodes, the cover gas pressure (p), and the duration of discharge (t). In wirebonding, these processes typically occur over very short time scales (~1 millisecond) and small length scales (~25 µm). Direct experimental observations of the process become very difficult. Cohen & Ayyaswamy[27] have performed a dimensional analysis to identify the principal dimensionless parameters governing such processes. These parameters are identified as wire diameter (d) to gap length ratio, $\frac{d}{G}$, Surface tension force to weight ratio, $\frac{3\sigma}{2\rho R^2 g}$, the discharge parameter, $\frac{I\Delta Vt}{pG^3}$, the pressure parameter, $\frac{p}{\rho g d}$, and the ratio of surface tension to electromagnetic body forces, $\frac{2\pi d\sigma}{JBv}$. In this case, $J = 4I/\pi d^2$ is the current density, B is the magnetic induction, estimated to be at most $\mu I/\pi d$, where, µ is the magnetic permeability, and v is the volume of the ball.

The researchers calculated these parameters for the real scale and for the laboratory (enalarged) scale. They found that the dimensionless parameters are of extreme size and they argue that the physical problem has already achieved its limiting form, insensitive to further variation in these parameters. Thus, precise correspondence on the two scales would be unnecessary.

Scaling gold up 60 x , which would be (barely) parametrically permitted, is prohibitively costly. For large length scale ball formation, copper was used. The researchers regarded all the dimensionless similarity parameters as having achieved their limiting solution state by virtue of their extreme size. The fineness parameter is weakly small (on the large scale) but the discharge is still between a wire and a plane. For larger balls of heavier metals, the surface tension parameter is only weakly large so that the ball is shaped like a pendent drop rather than a near perfect sphere. This is easily accounted for as a perturbation in the numerical solutions. With this minor exception, the researchers argue that their upscaled experimental realization of ball formation by electric discharge heating of the end of a wire closely corresponds to the real scale process. Clearly, fine details of the process are scale dependent. In performing a computational simulation, the authors found that the (boundary) condition on heat flux at the plasma-wire tip boundary is not known due to the empiricism in the energy "accommodation coefficient ." In the large scale experiments, the authors implanted fine wire thermocouples in the wire samples at two locations above where the ball is formed. Recording the transient temperature response during the discharge, the heat flux from the discharge plasma to the wire can be inferred as described in the next section.

3. Calculation of Heat Transfer up the Wire

An important part of this study is the determination of the heat transferred from the arc to the wire. The extent of the Heat Affected Zone (HAZ) is determined by the rate of heat transfer to the wire tip, and the heat flux along the axis of the wire. As described in a later section, thermocouples are used to obtain the transient temperature variation at two axial locations on the wire. The determination of the heat transfer by conduction up the wire, based on these temperature histories, involves the solution of the

© International Microelectronics And Packaging Society

transient heat transfer equation for the wire. The histories are applied as time dependent temperature boundary conditions for the heat transfer problem. The axial (one-dimensional) conduction, storage, and heat loss by convection and radiation from the surface of the wire segment during the discharge, are taken into account by a transient energy balance, of the form,

$$\frac{\partial T}{\partial t} = \alpha \frac{\partial^2 T}{\partial x^2} - \frac{P}{A\rho c_p}[\varepsilon\sigma(T^4 - T_a^4) + h_c(T - T_a)],$$

$$\text{for all x in (0,L), t in } (0,t_d) \tag{1}$$

where T(x, t) is the temperature at any location x along the axis of the wire at time t. x is measured from the location of the first thermocouple. This location is chosen such that, at the end of the discharge, it is located close to the neck between the ball and straight wire. The authors assume that the wire is slender enough for the radial temperature gradients to be considered negligible, facilitating a one-dimensional treatment. Constant properties are assumed to facilitate analytical solutions. In this case, t_d is the duration of the discharge and L is the length of the wire segment between the two thermocouple locations. T_a is the ambient temperature, and α, c_p and $\in$ are the thermal diffusivity, specific heat, and surface emissivity of the wire material, respectively. P and A are the perimeter and cross-sectional area of the wire. σ is the Stefan-Boltzmann constant and h_c is the convective heat transfer coefficient at the wire surface. To simplify the solution of the transport equation, the authors linearize the radiation term by employing the concept of a radiative heat transfer coefficient defined as follows,

$$h_r = \varepsilon\sigma\frac{T^4 - T_a^4}{T - T} = \varepsilon\sigma(T + T_a)(T^2 + T_a^2) \approx \varepsilon\sigma(\hat{T} + T_a)(\hat{T}^2 + T_a^2) \tag{2}$$

where $\hat{T}$ is the average temperature of the wire during the discharge. Combining the convective and radiative heat transfer coefficients, one can write,

$$h = h_c + h_r$$

For the duration of the discharge, the transient temperature variation is sufficiently accurately represented by a linear function of time as indicated by the temperature data obtained during the discharge process. Therefore, the initial condition and the boundary conditions are as necessary,

$$\text{at } t=0 \quad T(x,t) = T_a, \qquad \text{for all x in (0,L)} \tag{3}$$

$$\text{at } x=0 \quad T(x,t) = (T_{f0} - T_a)\frac{t}{t_d} + T_a, \qquad \text{for all t in } (0,t_d) \tag{4}$$

$$\text{at } x=L \quad T(x,t) = (T_{fL} - T_a)\frac{t}{t_d} + T_a, \qquad \text{for all t in } (0,t_d) \tag{5}$$

Here, $T_{f0} = T(0, t_d)$ and $T_{fL} = T(L, t_d)$ (6)

Next, the authors nondimensionalize the transport equation by defining the following non-dimensional (*) quantities.

$$\theta^* = \frac{T - T_a}{T_{f0} - T_a}, t^* = \frac{t}{t_d}, x^* = \frac{x}{L}, \tag{7}$$

where T_{f0} is the reference temperature. Then, the non-dimensional heat transport equation, and the initial and boundary conditions constitute the following boundary value-initial value problem.

$$\frac{\partial\theta}{\partial t} = F_o\frac{\partial^2\theta}{\partial x^2} - \left(\frac{4ht_d}{d\rho c_p}\right)\theta, \qquad \text{for all x in (0,1), t in (0,1)} \tag{8}$$

$$\text{at } t=0 \quad \theta(x,t) = 0, \qquad \text{for all x in (0,1)} \tag{9}$$

$$\text{at } x=0 \quad \theta(x,t) = t, \qquad \text{for all t in (0,1)} \tag{10}$$

$$\text{at } x=1 \quad \theta(x,t) = \frac{T_{fL} - T_a}{T_{f0} - T_a}t \equiv Kt(say), \qquad \text{for all t in (0,1)} \tag{11}$$

In the above, the asterisks for dimensionless quantities have been omitted for convenience. In this case, $Fo = \alpha t_d / L^2$ is the Fourier number.

Due to the presence of the time-dependent boundary conditions, the Laplace transform method is employed to solve the above fully transient formulation. For this purpose, the following transformation of the dependent variable θ is used.

$$\theta = \bar{\theta}e^{-Bt} \tag{12}$$

where $B = \frac{4ht_d}{d\rho c_p}$. The transformed problem then becomes,

$$\frac{\partial\bar{\theta}}{\partial t} = Fo\frac{\partial^2\bar{\theta}}{\partial x^2}, \qquad \text{for all x in (0,1), t in (0,1)} \tag{13}$$

$$\text{at } t=0 \quad \bar{\theta}(x,t) = 0, \qquad \text{for all x in (0,1)} \tag{14}$$

$$\text{at } x=0 \quad \bar{\theta}(x,t) = te^{Bt}, \qquad \text{for all t in (0,1)} \tag{15}$$

$$\text{at } x=1 \quad \bar{\theta}(x,t) = Kte^{Bt}, \qquad \text{for all t in (0,1)} \tag{16}$$

Performing a Laplace transformation over the time domain, $[t \to s]$ such that,

$$L\,[\bar{\theta}(x,t)] = \bar{\theta}(x,s)$$

The researchers obtained a second order differential equation in x with boundary conditions:

$$\frac{\partial^2\bar{\theta}}{\partial x^2}(x,s) - \frac{s}{Fo}\bar{\theta}(x,s) = 0,$$

$$\bar{\theta}(0,s) = \frac{1}{(s-B)^2},$$

$$\bar{\theta}(1,s) = \frac{K}{(s-B)^2},$$

The solution to this equation is of the form,

$$\bar{\theta}(x,s) = \frac{1}{(s-B)^2}[K\frac{\sinh qx}{\sinh q} + \frac{\sinh q(1-x)}{\sinh q}], \quad (17)$$

where $q = \sqrt{\frac{s}{Fo}}$. The temperature gradient in the transformed domain is written as follows,

$$\frac{\partial\bar{\theta}}{\partial x}(x,s) = \frac{1}{(s-B)^2}\{\frac{Kq\cosh qx}{\sinh q} - q\frac{\cosh q(1-x)}{\sinh q}\} \quad (18)$$

The researchers invert the Laplace transform using the Bromwich contour integral formula[28]. The transform has a second order pole at s = B and simple poles at $q = \sqrt{s/Fo} = in\pi$, where n = 1,2,3, . . . Employing Jordan's Lemma and Cauchy's residue theorem, one would obtain the Laplace inverse after some algebra[28]. Also, inverting the transformation $[\theta \rightarrow \bar{\theta}]$, one can obtain the following,

$$\begin{aligned}\frac{\partial\theta}{\partial x}(x,t) = {} & (t\hat{q} + \frac{1}{2\hat{q}Fo})[K\frac{\cosh\hat{q}x}{\sinh\hat{q}} - \frac{\cosh\hat{q}(1-x)}{\sinh\hat{q}}] \\ & + \frac{1}{2Fo}[Kx\frac{\sinh\hat{q}x}{\sinh\hat{q}} - (1-x)\frac{\sinh\hat{q}(1-x)}{\sinh\hat{q}}] \\ & - \frac{\coth\hat{q}}{2Fo}[K\frac{\cosh\hat{q}x}{\sinh\hat{q}} - \frac{\cosh\hat{q}(1-x)}{\sinh\hat{q}}] \\ & + \sum_{n=1}^{\infty}[1-(-1)^n K\frac{2n^2\pi^2 Fo}{(n^2\pi^2 Fo + B)^2}\cos n\pi x e^{-(n^2\pi^2 Fo+B}\end{aligned} \quad (19)$$

where $\hat{q} = \sqrt{B/Fo}$. The above instantaneous heat flux may be integrated over time at any location x. Thus, the cumulative heat flux up the wire is computed at x = 0. This is extrapolated to the wire tip to account for the transient energy storage in the segment that forms the ball. When this is multiplied by the wire cross-sectional area, one can obtain the heat transfer, Q_k, up the wire axis. This value of Q_k is added to the other heat quantities Q_m (heat of melting), and Q_{hr} (heat lost to convection and radiation from the tip) to obtain the total heat transfer, Q_w, to the wire. Next, a brief description of the experimental setup and procedure is provided, followed by results and discussion.

4. Experimental Setup and Procedure

In order to simulate the real scale conditions, a special enlarged (60x) capillary was constructed to deform the tips of the up-scaled wire samples (1.55 mm diameter) in exactly the same way as happens in wirebonding (see Figure 1). The up-scaled arc chamber is constructed of concentric cylinders of stainless steel tubing approximately 0.3 m high. The electrode holders are made up of two threaded hollow copper tubes. The threaded copper tubes are mated with similarly threaded machined copper fittings with receptacles to hold the electrode tips. An aluminum plug with a centered drilled hole to accommodate the 1.55 diameter copper wire is press fitted into the anode receptacle. The entire anode assembly can be pneumatically actuated. This facilitates arc initiation by electrode contact.

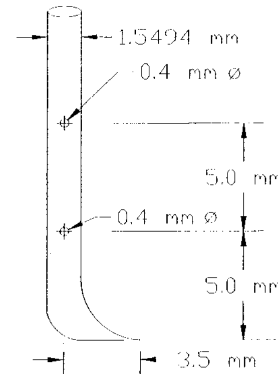

Figure 1. Wire sample drawing.

The cathode cylinder has a flat 1% thoriated tungsten tip. The arc chamber is evacuated to l0-15 mm Hg.The electrical equipment consists of a 40 kW, 90 V DC open circuit voltage power supply that rectifies a 480 V 3-ph ase, 60 Hz AC supply. An LC filter reduces the output ripple to less than 2% with the dominant frequency of 360 Hz. A 0 - 6 ohm variable ballast resistor placed in series with the arc current is used to control and vary the arc current. Data are recorded using a personal computer (PC) with a data acquisition (DAQ) board. This is supported by suitable software for data management, manipulation, and display. A 0.158 Ω resistor is placed in series with the arc current and a 56 kΩ/ 1.02 MΩ voltage divider is placed in parallel with the arc voltage so that both signals are reduced to a level that can be accepted by the data acquisition board. Fine wire (50.8µm) type K (Chromel-Alumel) thermocouples are used to measure the temperatures at two different locations along the length of the wire to obtain the transient thermal characteristics. The thermocouple hot junctions are cemented into 0.4 mm diameter through-holes at distances of 5 mm and 10 mm from the deformed tips of the wire samples. The depth of immersion of the thermocouples is about 0.5 wire diameter to minimize errors. As indicated by a simple parametric analysis, axial conduction is the predominant heat transfer mechanism. Therefore, experimental errors due to radial conduction are estimated to be less than 1%. A high temperature cement which has a high thermal conductivity but is electrically insulating is employed for this purpose. The thermocouple cold (reference) junctions are then soldered to thermocouple extension wires that pass through vacuum sealed holes in a removable plexiglass window of the arc chamber. The extension wires can either be connected through the cold junction compensator (hardware cold junction compensation) or directly (software cold junction compensation) to the amplifiers and then to the data acquisition board which is plugged into the PC. The output from the signal conditioning circuit is fed into analog input channels of the data acquisition board. Software routines using NIST (National Institute of Standards and Technology)

 © International Microelectronics And Packaging Society

polynomials convert the acquired signal to actual temperature values which may be post-processed as desired. The pressure in the arc chamber is sensed using a pressure transducer. A pair of relays enable the computer to control the switching of the DC power supply through a solenoid switch and the pneumatic cylinders (that actuate the anode) through a solenoid valve. This enables us to fully program the duration of the arc. A schematic of the experimental setup is shown in Figure 2.

Figure 2. Schematic of the experimental setup.

The experimental procedure is as follows. The arc duration is set in the PC software routines by the user. The discharge gap is set by controlling the displacement of the pneumatic actuator. At the start of the experiment, the anode wire sample and the cathode are in electrical contact.

The melt formation and resolidification of the wire tip consists of three software programmable steps. These are switching on the power, initiation of the arc by pneumatic controlled separation of the electrodes, and switching off the power. The time delay between the electrode separation and switching off the power is the arc duration. During the discharge, the software program records the voltage, current, temperature, and pressure data through the data acquisition board. The dimensions of the balls so formed are then measured. The balls are mounted, sectioned, polished and etched for metallographic examination. The etched ball sections and wire longitudinal sections are studied under an optical microscope. The microscope is also equipped with a Polaroid camera which is used to produce up to 40x magnified photographs of the etched sections. From the photomicrographs, the number and size of voids are measured to provide an estimate for the fraction of voidage. The accuracy of the voidage estimates also depend on the frequency of observations during grinding and polishing of the sections. The results for representative experimental runs are presented and the overall experimental study is discussed.

5. Results and Discussion

The series of experiments consisted of varying both the discharge current using the ballast resistor and adjusting the duration of the discharge to form the balls. The trials reported in this study were conducted at a chamber pressure of 11.6 mm Hg and fixed arc gap of 6.5 mm.

In Figure 3, the authors present the discharge current and discharge power histories for a mean discharge current of about 21 amperes. The horizontal axis indicates the time elapsed since the initiation of the experiment. As shown by the plots, the initial short circuit current of about 29.9 amperes rapidly decreases with electrode separation due to of electrical breakdown of the cover gas (air). The discharge current fluctuates rapidly about the mean discharge value until power is shut off, at which point it rapidly goes to zero. The discharge power is expressed as the product of the discharge current and the voltage. During the initial stage, the short circuit current results in a relatively small power consumption. Once the arc is initiated, the discharge power curve shows a peak andthen a series of fluctuations until power is shut off when the discharge power curve goes to zero. The voltage history also follows this chain of events with the voltage drop across the electrodes being zero in the initial short circuit then rapidly rises and fluctuates about a mean value of 37 V until power is shut off. At this point the voltage slowly dissipates as the capacitor bank in the LC circuit of the power supply discharges.

Figure 3. Current & power transient variations.

The corresponding temperature histories for the same run as Figure 3 at locations 5 and 10 mm from the deformed wire tip are presented in Figure 4. As may be anticipated, after the initia-

tion of the discharge, the arc discharge generates a large amount of heat and a part of it is deposited at the tip of the wire which melts the tip. The large temperature differential along the wire generates a temporally increasing conductive heat flux along the axis of the wire. This is indicated by the increasing temperatures recorded by the thermocouples.

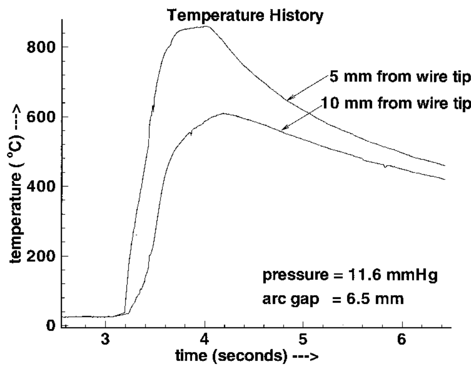

Figure 4. Temperature transient variation.

In Figure 5, a photomicrograph (50x) of the etched ball section is shown for a run with a mean discharge current of 12.9 A. The authors note the columnar grains formed due to the nature of the solidification process. Once the arc discharge is terminated, the heat flux at the ball surface almost instantaneously reverses direction as heat from the melt is lost by natural convection and conduction to the surrounding air. A few surface layers in this region get instantaneously quenched leading to a surface layer of very fine grains. However, the primary heat loss mechanism from the ball is still the heat conduction along the axis of the wire. Therefore, the solidification front progresses almost normal to the axis of the wire downwards away from the end of the melt region at the wire towards the interior of the ball. This has also been borne out in the recent studies by Huang et al.[12] and Cohen et al.[25] with an initially undeformed wire. This explains the columnar grains indicated in the figure. The line between the columnar grain region and the polyhedral grains indicates the location of the end of the melt region. In the photomicrograph, the authors can see evidence of some voids and a small amount of necking at the melt circumferential interface. From the photomicrographs and from observations made during the sectioning of the samples, the researchers are also able to estimate the void content for each ball. The ball shown in Figure 5 was deformed from sphericity by its weight. Clearly, a real scale copper ball would be (nearly) perfectly due to the extreme dominance of surface tension over gravity forces.[29] The voids that are visible also are due to the 60x enlargement of the experiment. These numerical simulations of solidification of molten balls showed that on the real (25 μm) scale conduction up the wire axis is so dominant that any potential shrinkage void would be pushed out the bottom of the ball before solidification. However, on the large scale, it is possible that there is just enough cooling through the sides of the ball to trap a shrinkage void within. In these two respects, Figure 5 does not represent a valid model of a real scale ball.

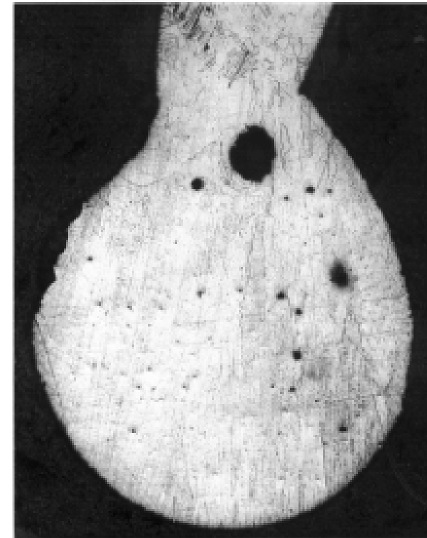

Figure 5. Photomicrograph of etched ball section.

In Figure 6, the authors present the photomicrograph of the etched wire longitudinal section for the same run as Figure 5. The section is at a distance from the ball which displays the extent of the Heat Affected Zone (HAZ). In the lower half of the picture, the grains are equiaxed and the grain boundaries are well defined. In the upper region, the grains are less defined and etch darkly. These observations lead to the conclusion that the lower part of the Figure which is toward the ball consists of recrystallized grains while the upper region of the figure corresponds to relatively unaffected regions. This indicates the extent of the HAZ relative to the ball. The researchers have recorded the extent of the HAZ for all the samples.

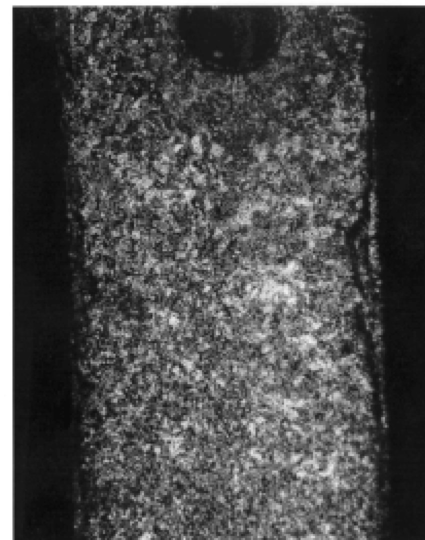

Figure 6. Photomicrograph of etched wire.

© International Microelectronics And Packaging Society

The temperature histories and measured ball dimensions are used to calculate the time averaged arc heat transfer to the wire tip/ball during the discharge process. The method of calculation of the heat transfer is similar to that described by Cohen et al.[25] The authors summarized the method as follows. From the temperature history, one can compute the average heat transfer, Q_k, along the axis of the wire during the discharge as described in an earlier section. The latent heat of fusion is used to compute the energy of melting Q_m. The ball also undergoes heat loss by convection and radiation Q_{hr} to the surrounding air. The three quantities may then be summed to obtain the net heat input Q_w to the wire tip/ball. The integral of the power (IV) over the discharge duration gives the electrical energy, Q_a, consumed by the arc. The ratio of the heat input to the ball to the electrical energy consumed gives the fraction of the total energy consumed in ball formation. In Table 1, the researchers present the various heat quantities and the ratio of the heat input to the wire to the electrical energy consumed (Q_w/Q_o) f or various values of average discharge currents and the corresponding arc durations t. The values represent calculations averaged over four runs at each setting in the arc chamber.

Table 1. Heat quantities for various currents.

I_{av} (A)	t (sec)	Q_w (J)	Q_a (J)	Q_w/Q_a
5.80	0.832	75.03	229.2	0.327
11.6	0.302	125.9	221.3	0.569
12.9	0.457	80.13	205.1	0.391
17.5	0.137	33.93	88.19	0.385
21.0	0.360	86.04	280.4	0.307

Figure 7 shows the variation of the voidage (volume void fraction) with the average discharge current (four runs at each current value) The curve shown is a parametric spline fit through the data. The trend in voidage shows a dramatic change because of the appearance of large shrinkage voids at the center of the ball for higher values of the discharge current. As noted above such voiding does not occur on the real scale. We report it here because it was an outcome of our experiments. In Figure 8, we present the variation in the length of the HAZ along the axis of the wire (referred to the tip of the bent wire) and non-dimensionalized by the wire diameter. The HAZ length shows a decreasing trend with increasing current. As the current increases, the arc duration required to form a ball decreases. This in turn implies there is less time available for heat effects (e.g. grain recrystallization) to penetrate axially along the wire away from the ball. Due to the finite thermal diffusivity of the metal, this would in turn imply the length of penetration of heat effects or the extent of HAZ would also decrease with higher currents.

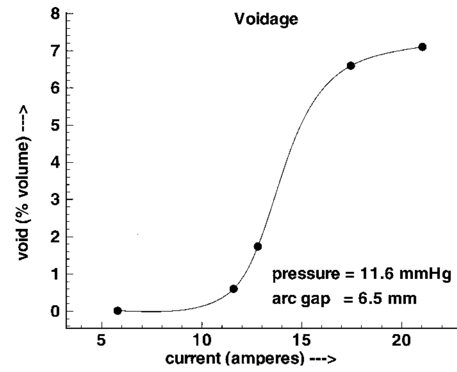

Figure 7. Variation of voidage with current.

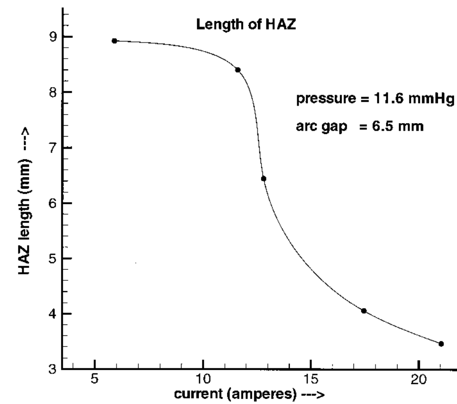

Figure 8. Variation of HAZ with current.

The voidage and HAZ variation are shown with current as the independent variable because, current is the major control variable in the discharge process.

6. Experimental Uncertainties

The uncertainty in the discharge voltage and current measurements is ±1.5%. The uncertainty in the thermocouple temperature is 2.2 °C or ±0.75% whichever is greater. The uncertainty in the temperature time history also depends on the response time for the thermocouples. The thermocouple response time is characterized by the rated time constant. The time constant leads to an estimated uncertainty of ±3.5% in the transient response for the experiments. An error analysis indicates that uncertainty in the heat flux calculations is ±4.2% due to propagation of uncertainties in measured data. The uncertainty in the HAZ length measurement is ±2%. The maximum uncertainty is in the voidage estimates and is ±7%.

7. Conclusions

The authors have made a comprehensive experimental and numerical study of the heat transfer associated with an electronic flame off discharge process used in microelectronic packaging. To simulate industrial situations, 60x enlarged scale bent wire samples were fabricated using a special capillary. The samples were used in the arc chamber and the discharge current was varied as the independent variable while keeping the pressure and arc gap constant. The entire discharge process is programmable through a personal computer.

Discharge current and voltage histories and characteristics were obtained. Implanted fine gage thermocouples were employed to obtain the temperature histories at two locations along the axis of the wire. The temperature histories and ball size measurements enabled the researchers to estimate the heat input to the wire. The balls so formed were also analyzed metallographically and representative photomicrographs have been presented. From the micrographs, estimates of the void content and extent of the Heat Affected Zone (HAZ) were obtained and have been presented. In order to form "good" balls, lower void content is desired. This limits the magnitude of the discharge current. However, owing to the demands for low chip profiles and consequently low wire loop heights, the HAZ length needs to be minimized. This requires higher discharge currents. These opposing trends of voidage and HAZ lengths with discharge current may be optimized to give the "best" design settings that would lead to "good" balls.

Acknowledgments

The authors gratefully acknowledge support of this work by the National Science Foundation through NSF Grant CTS-94-21598 including the REU Supplement (which supported undergraduate students L. Medalla and B. J. Mulada during the summer of 1996). They are also grateful to the Research Foundation of the University of Pennsylvania for the generous grant of an IBM RS/6000 machine on which many of the calculations presented in this work were performed.

References

1. J. D'Ignazio, "Wirebonding's Reign Continues," *Semiconductor Int.*, Vol. June, pp. 117-126, June 1996.
2. A. J. Otto, "Aluminum wire for ball bonding," *Proceedings of the 37th Electronic Components Conference*, CHMT Division, IEEE, pp. 550-556, 1987.
3. D. Baker and I. E. Bryan, "An improved form of thermocompression bond," *Br. J. Appl. Phys.*, Vol. 16, No. 6, pp. 865-871, 1965.
4. K. I. Johnson, M. H. Scott and D. A. Edson, "Ultrasonic wire welding: Part II: Ball-wedge wire bonding," *Solid State Technol.*, Vol. 20, No. 4, pp. 91-95, 1977.
5. B. L. Gehman, "Bonding wire microelectronic interconnections," *IEEE Trans. on Components, Hybrids, and Manufacturing Tech.*, Vol. 3, No. 3, pp. 375-383, 1980.
6. A. Bischoff and F. Aldinger, "Ball bonding with low cost ultrafine wires," *in Proc. 32nd Electronic Components Conf.*, CHMT Division, IEEE, pp. 254-261, 1982.
7. B. L. Gehman, K. E. Ritala and L. C. Erickson, "Aluminum wire for thermosonic ball bonding in semiconductor devices," *Solid State Technol.*, Vol. 26, No. 10, pp. 151-158, 1983.
8. G. McGill, I. M. Weilerstein, R. Venkatesh and J. Keverian, "Aluminum wire as a viable alternative to gold for ball bonding," *Semiconductor International*, Vol. June, pp. 91-95, August 1983.
9. J. Onuki, M. Suwa, T. Iizuka and S. Okikawa, 'Study of Aluminum ball bonding for semiconductors," *in Proc. 34th Electronic Components Conf.*, CHMT Division, IEEE, New Orleans, LA, pp. 7-12, 1984.
10. J. Kurtz, D. Cousens and M. Dufour, "Copper wire bonding," *in Proc. 34th Electronic Components Conf.*, CHMT Division, IEEE, New Orleans, LA, pp. 1-6, 1984.
11. J. Hirota, K. Machida, T. Okuda, M. Shimotomai and R. Kawanaka, "The development of copper wire bonding for plastic molded semiconductor packages," *in Proc. 35th Electronic Components Conf.*, CHMT Division, IEEE, pp. 116-121, 1985.
12. K. Atsumi, T. Ando, M. Kobayashi and O. Usuda, "Ball bonding technique for copper wire," *in Proc. 36th Electronic Components Conf.*, CHMT Division, IEEE, pp. 312-317, 1986.
13. L. Levine and M. Scheaffer, "Copper ball bonding," *Semiconductor International*, Vol. August, pp. 126- 129, August 1986.
14. G. G. Harman, *"Wire Bonding in Microelectronics"*, ISHM, Reston, VA, 1989.
15. L. J. Huang, "Fundamental Problems in Heat Transfer and Fluid Mechanics of Phase Change Processes with Liquid Drops," *Ph.D. Thesis*, Univ. of Pennsylvania, Philadelphia, Pennsylvania, 1989.
16. D. J. Vacek and I. M. Cohen, "Model of a Wire-to-Plane Electric Arc," *J. Appl. Phys.*, Vol. 65, pp. 1005-1008, 1989.
17. L. J. Huang, K, Ramakrishna, P. S. Ayyaswamy and I. M. Cohen, "An analysis of shrinkage porosity in Aluminum ball bonding process," *ASME Journal Electronic Packaging*, Vol. 111, No. 3, pp. 199-206, 1989.
18. L. J. Huang, K. M. Yu, S. Powell, I. M. Cohen and P. S. Ayyaswamy, "Ball formation in wire bonding, Part I: Upscaled experimental study," *International Journal for Hybrid Microelectronics*, Vol. 13, No. 1, pp. 1-5, 1990.
19. S. C. Chang, I. M. Cohen, L. J. Huang and P. S. Ayyaswamy, "Ball Formation in Wire Bonding, Part II: Real Scale Experimental Study," *International Journal for Hybrid Microelectronics*, Vol. 13, No. 2, pp. 29-34, 1990.

 © International Microelectronics And Packaging Society

20. L. J. Huang, M. A. Jog, I. M. Cohen and P. S. Ayyaswamy, "Effect of polarity on heat transfer in ball formation process," *ASME J. Electronic Packaging*, Vol. 113, pp. 33-39, 1991.
21. K. G. Donovan and I. M. Cohen, "Two-dimensional analysis of electrical breakdown between a wire and a plane- extended," *J. Appl. Phys.*, Vol. 70, pp. 4132-4138, 1991.
22. M. A. Jog, I. M. Cohen and P. S. Ayyaswamy, "Breakdown of a Wire-to-plane Discharge," *Phys. Fluids B*, Vol. 3, pp. 3532-3536, 1991.
23. M. A. Jog, I. M. Cohen and P. S. Ayyaswamy, "Electrode Heating in a Wire-to-plane Arc," *Phys. Fluids B*, Vol. 4, pp. 465-472, 1992.
24. L. J. Huang, P. S. Ayyaswamy and I. M. Cohen, "Melting and Solidification of Thin Wires: a -Class of Phase-change Problems with a Mobile Interface-I. Analysis," *International Journal of Heat and Mass Transfer*, Vol. 38, No. 9, pp. 1637-1645, 1995.
25. I. M. Cohen, L. J. Huang and P. S. Ayyaswamy, "Melting and Solidification of Thin Wires: a Class of Phase-change Problems With a Mobile Interface-II. Experimental confirmation," *International Journal of Heat and Mass Transfer*, Vol. 38, No. 9, pp. 1647-1659, 1995.
26. W. &in, I. M. Cohen and P. S. Ayyaswamy, "Non-equilibrium simulation of ball formation from a bonding wire: An application in microelectronic interconnection," *Symposium on Thermal Science and Engineering in honor of Chancellor Chang-Lin Tien*, Univ. of California, Berkeley, California, U. Illinois, pp. 365-371, Nov. 14 1995.
27. I. M. Cohen and P. S. Ayyaswamy, "Ball Formation Processes in Aluminum Bonding Wire," *Solid State Technology*, Vol. 28, No. 12, pp. 89-92, 1985.
28. D. G. Duffy, Transform Methods for Solving Partial Digerential Equations, CRC Press, Boca Raton, 1994.
29. S. S. Sripada, "Fundamental Studies of Plasma Applications in Microelectronic Manufacturing and Flames: Fluid Mechanics, Phase-change, and Heat Transfer," *Ph.D. Thesis*, Univ. of Pennsylvania, Philadelphia, 1999.

About the authors

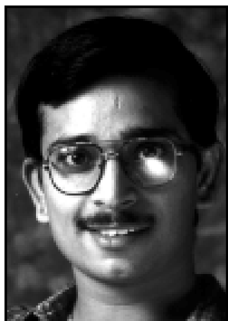

Srinivas S. Sripiada earned a Bachelors Degree with honors in Mechanical Engineering from the Indian Institute of Technology, Kharagpur, India, in 1993, a Masters Degree in 1995, and a Ph.D. in Mechanical Engineering & Applied Mechanics from the University of Pennsylvania, in 1999. Since February 1999, he has been employed as an Applications Engineer at i2 Technologies, Irving, TX working on manufacturing operations and planning optimization in the semiconductor manufacturing industry. Dr. Sripada's doctoral dissertation focused on the electronic flame off discharge process for ball bonding from a computational modeling as well as an experimental perspective.

Ira M. Cohen earned a Bachelors Degree in Aeronautical Engineering from Polytechnic Institute of Brooklyn, New York, in 1958, and a Ph.D. in Aeronautical Engineering from Princeton University in 1963. He was a member of the engineering faculty at Brown University from 1963-66. Dr. Cohen lectured in Europe and spent three summers doing research at Sandia National Laboratories in Albuquerque, New Mexico. He joined the faculty of the University of Pennsylvania in 1966, has been professor of mechanical engineering since 1976, and served 5-1/2 years as Department Chairman. For the past 15 years, he has devoted his attention to packaging problems in microelectronics – especially those related to ball formation and bonding.

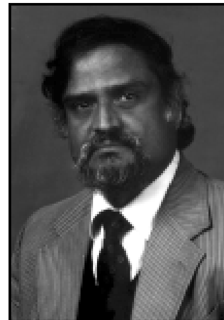

P. S. Ayyaswamy earned a Ph.D. in Engineering in 1971 from the University of California, Los Angeles, following a M.S. from Columbia University and a B.E. from the University of Mysore. From 1971 – 1974, he was a post-doctoral scholar at UCLA. He then joined the faculty of the University of Pennsylvania where he rose through the ranks and now is the Asa Whitney Professor of Dynamical Engineering. His research interests are in the fields of heat and mass transfer, with particular emphasis on convective and phase change heat transfer. He is the recipient of two awards for excellence in teaching and the Outstanding Faculty Advisor Award of the ASME. Part of his research has been dedicated to problems of heat transfer in ball formation since 1985.

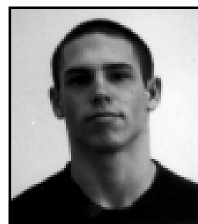

Leonor Medalla and Brian Mulada were undergraduate students who were supported by an NSF REU supplement during the summer of 1996. They graduated from the University of Pennsylvania with B.S.E. Degrees in 1998. Leonor Medalla is now working for Lockheed-Martin Electronics & Missiles in Orlando, Florida. Brian Mulada is in investment banking with Morgan Stanley Dean Witter in Menlo Park, California.